Peer-reviewed version available at Photonics 2018, 5, 11; doi:10.3390/photonics5020011

Article

Broadband Terahertz Light-Matter Interaction Enhancement for Precise Spectroscopy of Thin Films and Micro-Samples

Romain Peretti [1,*], Flavie Braud[1], Emilien Peytavit[1], Emmanuel Dubois[1] and Jean-François Lampin[1]

[1] IEMN, CNRS, Univ. Lille, Villeneuve d'Ascq, 59652, France;
* Correspondence: romain.peretti@iemn.univ-lille1.fr

Abstract: In biology molecules and macromolecules like sugars, proteins, DNA, and RNA are of utter importance. Detecting their presence as well as their conformation is still a challenge in many cases. It is well known that the vibrational states of such molecules lie from the infrared to the TeraHertz range. Spectroscopy can be used to detect such compounds and probe their conformation. Still, terahertz spectroscopy on biosample is a challenge for two main reasons: water absorption; and the small size of the samples. The sample volume is smaller than the cube of the TeraHertz wavelength; the light matter interactions are thus extremely reduced. In this paper, we present the design, fabrication, characterization and the first typical uses of a biophotonic device aiming at increasing light matter interaction to enable terahertz spectroscopy of minute samples on a broad band (0.2–2 THz). We demonstrate time domain spectroscopy experiments on few µl samples showing the validity of our approach.

Keywords: biophotonic; Terahertz; time domain spectroscopy; absorption enhancement; laser cutting

1. Introduction

Confining light in a small volume increases light-matter interactions as described in Purcell's theory. Such enhancements are useful for nonlinear optics, laser and for detection purpose especially when one wants to make light interact with a small object as molecules or bio samples. In these latter cases, the refractive index of the samples and their environment (substrates, matrices, solvents …) are often relatively low. In material with high refractive index, light confinement is now accessible using, for instance, photonic crystals. However, confining light in a low refractive index is still a challenge in several spectral ranges. In the visible or near infrared, dielectric structure had been proposed [1, 2, 3] showing interesting results but the achieved volumes remained at the order of magnitudes of the cube of the wavelength. The main approaches to reach smaller sizes are to use metallic structures using plasmonic effects [4, 5, 6] and lead to several breakthrough but with the intrinsic drawback of bringing additional losses.

Terahertz technology has shown an increasing development in the last years. If almost the entire electromagnetic (EM) spectrum is being used, one spectral range has still to be harnessed and exploited, namely, the Terahertz band. Because of its application in security and healthcare, THz domain is nowadays one of the most appealing spectral ranges. There, many materials and living tissues are semi-transparent, and can be imaged, identified, and analyzed. THz range is, extremely promising in spectroscopy especially for biologic systems since the energy of the photon in the THz range is around the one of $[k_B \times T]$ at room temperature (~6 THz) and to the one of the fundamental vibrational modes of molecules, molecular crystals and macromolecules like carbohydrates[7], DNA, RNA, proteins [8] … To summarize, if spectroscopy in the mid infrared range of the spectrum probes

Peer-reviewed version available at Photonics 2018, 5, 11; doi:10.3390/photonics5020011

mainly vibrations associated to localized atom-atom stretches in molecules, THz frequency probes mainly collective vibrational modes in heavy and/or long molecules. However, there are still many hurdles to jump over to fully and practically enable THz spectroscopy on actual biosamples. One of the major ones is that they are very small compared to the THz wavelength, which is typically in the range between 0.1 and 1 mm. It is then mandatory to enable subwavelength confinement of the THz electromagnetic field in the sample.

Such confinement has been a subject of interest in the community. To our knowledge, all the approaches take the benefits of the relatively good quality of metals in the THz compared to visible or near infrared ranges. There are two different approaches. The first one is using near-field microscopy set-up and enabling THz spectroscopy on it [9]. The second one is using subwavelength waveguide structure. One can for instance uses a metallic wire [10] around which the THz wave will propagate ant then deposit on it the substance to probe. There, the light matter interaction is not fully enhanced, because higher confinements can be achieved using full metallic boundary conditions. The most natural approach to confine in one direction is to use a parallel plate metallic waveguide (PPMW) [11]. Indeed in such a waveguide the lower frequency mode (Transverse Electro Magnetic : TEM) shows no frequency cut-off, relatively low losses and, importantly, a very weak dispersion only linked to the metallic material dispersion, which is ideal for time domain spectroscopy (TDS) [12, 13] experiments. However, a specific coupling scheme is needed to properly excite the mode of interest. The first method uses silicon cylindrical lenses [11] with the drawback of introducing a coupling highly dependent on the waveguide geometry and additional reflections due to the high refractive index of silicon. Still, this technics was used even inside a cryostat [14]. To overcome these limitations, tapered coupling antennas were used [15] and allowed to improve the coupling and the ease of use of such a device. However, the main limitation of the PPMW is that it assumes a quasi-infinite height with a major consequence that there is no vertical confinement. There are two drawbacks to this; first, the light matter interaction on small samples would be smaller than in the case of 2D confinement; second, no vertical confinement means that during the propagation inside the waveguide, the mode will expand in the vertical direction resulting in a strong astigmatism probably explaining the high losses experienced in [15].

In this article, we present the design, the technological process, the characterization and a typical application of a device aiming at confining THz pulses into a 2D waveguide. This thick slot line waveguide (TSLW) does not show significant reflection and dispersion. We combined the curved tapered antenna approach similarly to [15] to inject properly the beam into our waveguide together with the approach of [[] using a fully planar geometry and a subsequent 2D confinement. We modified this combination with exponential grown as in Vivaldi antennas. Due to its final shape and geometry, we named our exponential tapered antenna coupled metallic waveguide as "*Butterfly*".

2. Design

1.1. General considerations

There are four aims for our butterfly device. (1) The hollow guiding part, where the THz-light will be confined and the light matter interaction enhanced should be long enough (several mm meaning several tens of wavelengths). (2) The hollow part had to remain accessible from the outside in order to enable filling the slot with an analyte. (3) One has to be able to inject and extract light from it using standard THz optical lenses or mirrors. Finally, (4) the device should not induce significant dispersion nor echo pulses resulting from any reflection.

Translating these requirements in components gives: (1) & (2), we need a waveguide with a cross section at the wavelength scale, which is not closed. (3) & (4) we need one non-dispersive and matched antennas for injection and for extraction of the THz pulse. We decide to use a planar design to fulfill (2) & (3) and to fulfill (4) we limit our toolbox to the use of the transverse electromagnetic mode of a metallic quasi-coplanar waveguide. Thus, we decide to use a device made of three components: an injection exponentially tapered antenna (ETA) [17], a TSLW [18] and an extraction exponentially tapered antenna making the butterfly shown in Figure 1.

Preprints (www.preprints.org) | NOT PEER-REVIEWED | Posted: 26 February 2018 doi:10.20944/preprints201802.0157.v1

Peer-reviewed version available at Photonics 2018, 5, 11; doi:10.3390/photonics5020011

Indeed, the TSLW can be seen as the intermediate topology between the parallel plate waveguide [19, [] and the slot line waveguide [18]. In the case of absence of any substrate, both are known to support a TEM mode, and thus have a very small dispersion [20, 21] even up to optical wavelengths [22].

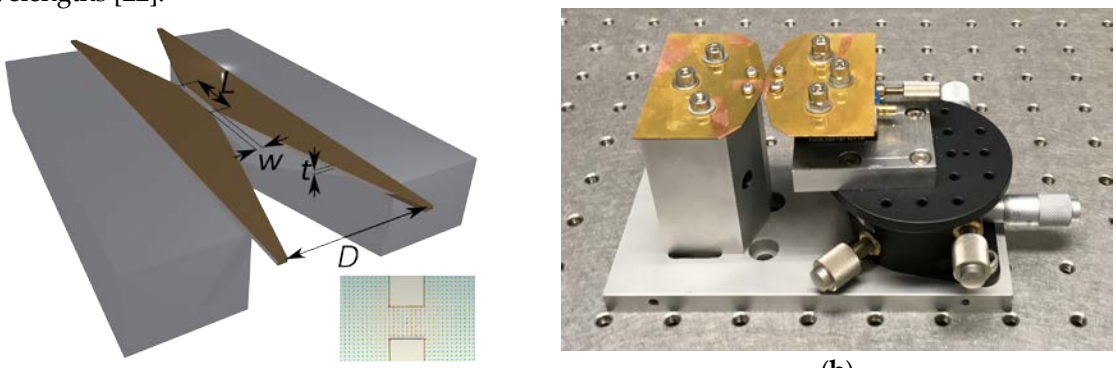

(**a**) (**b**)

Figure 1. (**a**) Schematic of the butterfly showing the main parameters (the inset depicts the field in the waveguide); (**b**) picture of the realization of the butterfly on its holder with micrometer screws.

We choose the thickness t of the TSLW (and the metallic plate) to be 500 μm, thick enough to insert a sample in and thin enough to confine the THz field and we keep the width w as the variable since we will put one of the wing of the butterfly on top of a micrometer displacement stage. We choose the length L to be 10 mm, which is a relatively large value for THz solid-state sample but will allow evaluating the losses of such butterfly device.

The exponentially tapered antenna [17] was chosen to avoid reflections at the guide/ antenna interface by keeping a continuous curve with continuous derivative giving a shape following the parametric equation in s:

$$\begin{bmatrix} x \\ y \end{bmatrix} = \left[\beta\left(\exp\left(\frac{s}{\alpha}\right)-1\right)\right]\begin{bmatrix} \cos(\theta) & -\sin(\theta) \\ \sin(\theta) & \cos(\theta) \end{bmatrix} = \begin{bmatrix} s\cos(\theta)-\sin(\theta)\,\beta\left(\exp\left(\frac{s}{\alpha}\right)-1\right) \\ s\sin(\theta)+\cos(\theta)\,\beta\left(\exp\left(\frac{s}{\alpha}\right)-1\right) \end{bmatrix} \quad (1)$$

Where $\theta = -\operatorname{atan}\left(\frac{\beta}{\alpha}\right)$ to keep the curve derivative continuous at the interface with the waveguide (α and β are the two parameters for the exponential). More concretely, α is a length depicting how fast the exponential will end up following its asymptotic linear curve. In other words, the higher is α, the smoother and longer will be the exponential region. Consequently, it will introduce uncertainty on the actual length of the waveguide. Additionally θ gives the opening angle of the antenna away from the waveguide. This is how we fixed and α to 10 μm and β to 30 μm. This curve is repeated 4 times following the x and y symmetry of the butterfly.

As a validation for our approach, we performed Electromagnetic, time domain simulations using CST software [23].

1.2. Waveguide simulation

As stated before, the TSLW lie between the parallel plate's waveguide and the slot line waveguide. In the first case, the plates are the vertical sidewalls of the wings, in the second case the slot is the void between the wings. Since we aim at using low dispersion modes, we will focus on the transverse Electromagnetic mode (TEM). As material, we used lossy metal with the DC conductivity of copper. The losses are a combination of the ohmic losses in a parallel plate's waveguide [19]:

$$\gamma'' = \sqrt{\frac{\omega\epsilon}{2\sigma}}\frac{1}{w} \quad (2)$$

, with additional losses due to finite size thickness. The results are shown in fig 2

Preprints (www.preprints.org) | NOT PEER-REVIEWED | Posted: 26 February 2018 doi:10.20944/preprints201802.0157.v1

Peer-reviewed version available at Photonics 2018, 5, 11; doi:10.3390/photonics5020011

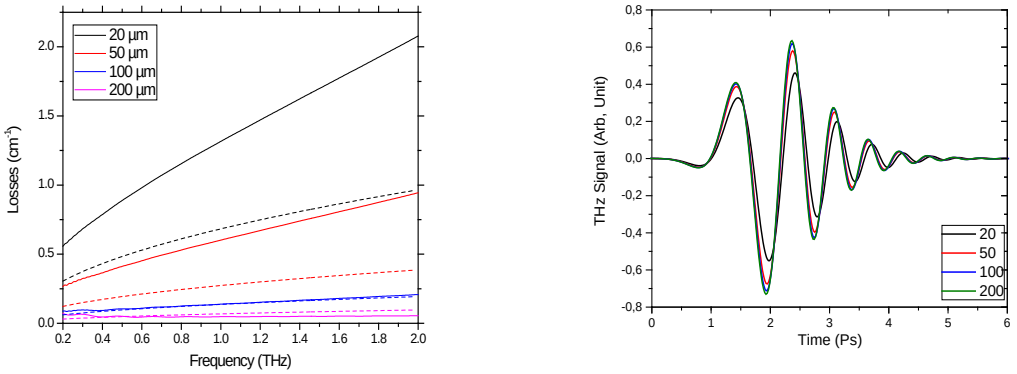

(**a**) (**b**)

Figure 2. (a) Theoretical losses (dashed lines) compared to simulated ones (surface conductance of 5.96 10^7). Difference between them for 20 and 50-µm wide waveguide are given in dotted lines **(b)** Electric field pulse after propagating through the 5 mm waveguide for several widths.

As seen, the losses are reversely proportional to the width of the waveguide. Considering the fact that simulations of the same structure with perfect electrical conductor instead of conductive cooper were performed and did not show significant losses, one can conclude that all the losses origin from ohmic losses from the metal. One can see discrepancy between the theoretical parallel plate's waveguide: losses with the simulated ones. The additional losses in simulation show a linear behavior with frequency. Since in infinitely thick and in infinitely thin SLW [24] are known to show a square root dependency with frequency, we attributed it to the finite nature of the thickness of the metal. One can similarly observe these losses on the time domain data (after 5 mm waveguide). In addition, these data show negligible dispersion (the pulse is not broadened). These simulations confirm the choice made for the waveguide regarding our goal.

1.3. Antenna simulation

Now that the waveguide fulfills our requirements, we have to couple it to free space using antenna. The additional constraints of being low dispersion, broadband and planar build our choice of antenna presented above. The two main characteristics of the antenna in our problem will how the couple THz-light into the waveguide and how they couple light into free space. Thus we looked over the reflection (S_{11} parameter of the dominant mode) and the far field pattern of a 1 mm long and 20 µm wide waveguide followed by a TSLW with the above mention parameter with an opening D=500µm. This value for D is rather small but we cannot perform simulations for larger D due to the amount of memory needed. Still these simulations allow to understand the behavior of the antenna and to draw the main conclusions.

The S_{11} parameter is shown on fig 3.

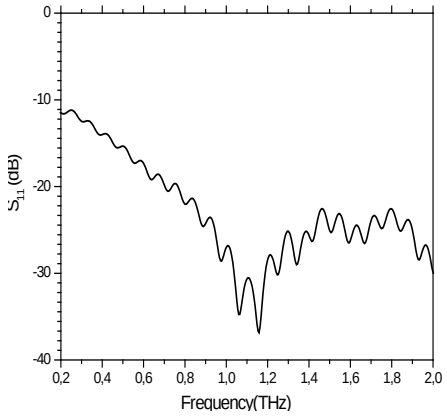

Figure 3. Reflection coefficient **S_{11}** versus frequency in dB for a D=500µm w=50 µm L=1 mm.

Preprints (www.preprints.org) | NOT PEER-REVIEWED | Posted: 26 February 2018 doi:10.20944/preprints201802.0157.v1

Peer-reviewed version available at Photonics 2018, 5, 11; doi:10.3390/photonics5020011

This figure shows two different behaviors depending on the frequency range on top of which a Fabry-Perot effect induces a modulation. At low frequency there is an exponential decay of the S_{11} coming from the size of the simulated antenna reaching saturation at higher frequency than 1.2 THz. The value for reflection at low frequency is too high for our requirements. However, the value is fully compatible when it reaches the saturation. This means that for the simulated size of antenna (D=500µm) an important part of the spectrum could not be use. However since this value of D is only limited by the memory needed in the simulations and since all the simulations are scalable, we will have this cut-off value around 12 GHz for D= 5 cm.

To go a step further we computed the far field of the described antenna. Due to memory limitation, the ratio between the aperture D and the wavelength was limited to 8 which is small compare to the realization (ratio between 30 and 300). We plotted the results in fig 4. It is important to notice that the width of the waveguide did not change the far field pattern since we feed the guide always with the same mode of interest.

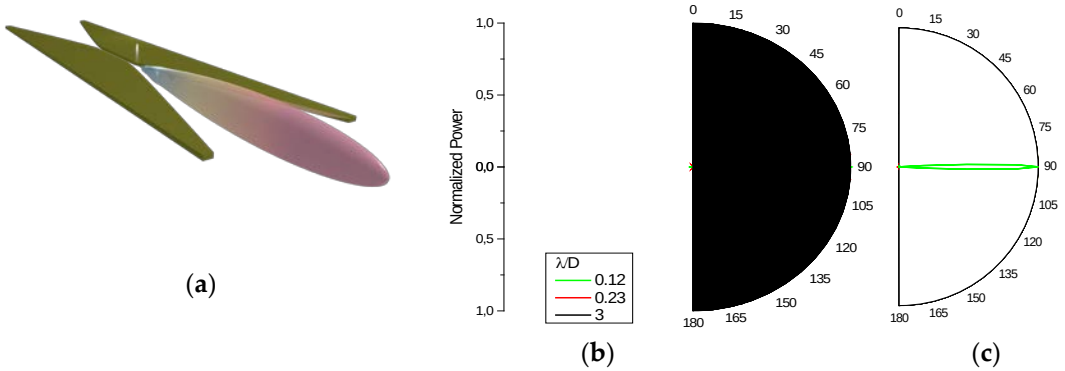

Figure 4. Far field radiation patterns in power (linear scale). (**a**) 3D view at 2.6 THz (λ/D=0.23) (**b**) E-plane radiation pattern (horizontal cross section) at 0.2, 2.6 and 5THz (λ/D=3; 0.23; 0.12) **(c)** H-plane radiation pattern (vertical cross section). The golden areas depict the geometric asymptotic opening angle of the metal plates.

First, one can see on fig 4a that the radiation pattern has a single main lobe pointing along the waveguide axis. To be quantitative figure 4 b and c show two sections of the radiation pattern, respectively the E-plane and the H-plane. These two graphics show that at very low frequency ($\lambda > D$) the radiation pattern is too wide and has several lobes, making it unusable. However, for higher frequencies ($\lambda < D$) the radiation pattern is more directive and corresponds to the needs. More precisely the 3 dB half beamwidth for λ =0.12 D is 3° in the E-plane and 2° in the H-plane which is not perfectly axisymmetric but still usable for our application.

We decided to fabricated the butterfly with the following parameter, t=500µm, D=50mm and L=10 mm. This gives a λ =0.12 D frequency around 50 GHz which is far below the lower frequency of the TDS system (200 GHz) granting that the full pulse spectrum will be inside the butterfly bandwidth.

3. Technological process

3.1 Laser cutting

The fabrication of the butterfly assembly was realized by cutting each wing separately in a 500 µm thick copper plate. As shown in Fig. 1, one wing is mounted on a fixed stand while the second one is attached to a linear micrometre displacement stage to adjust the slot width. To properly achieve wing cutting, several demanding prerequisites must be fulfilled: i) first, the cutting process must be capable to describe complex curved trajectories, in particular the tapered exponential profile of antennas; ii) secondly, the cut sidewalls must be vertical to match the TSLW geometry; and iii) finally sidewalls must be burr-free and with a roughness level well below the working wavelength to avoid ohmic losses and propagation scattering effects. Over the past decade, short and ultra-short pulse lasers have gained widespread acceptance for industrial use ranging from micromechanics to semiconductor dicing, engraving or drilling [25]. When compared to blade dicing, laser ablation

brings more accuracy with a micrometre-sized spot resulting in extremely narrow and low roughness kerf lines. It furthermore does not require a cooling fluid during operation. Another distinctive advantage of laser cutting ensues from being a maskless technology suitable for complex cutting patterns and fast prototyping cycles, thus reducing complexity and cost. Among pulse laser sources, femtosecond ablation offers the additional merit of being a quasi athermal process that involves local sputtering instead of melting, boiling and evaporation. This results in much cleaner process with a negligible heat affected zone (HAZ). The laser setup used to cut wings in copper plates leverages a Tangerine laser source from Amplitude-Systèmes that generate ~350fs pulses at an infrared wavelength of 1030nm. The laser beam trajectory is controlled using a galvanometric scanning head followed by a final telecentric focusing lens featuring a focal distance of 100mm. The focused spot diameter is estimated around 10 μm at the considered wavelength. An optical attenuator comprising a half-wave plate and a polarizer allows fine tuning of the beam power independently from the laser source parameters. After crossing the entire optical path, the maximum available average power amounts to 12W at a repetition rate of 200 kHz. Copper cutting was performed under the following conditions after optimization: i) average power set to 100% (12W), ii) scanning speed adjusted to 20 mm/s, iii) repetition rate of 200 kHz and iv) 150 laser beam passes.

3.2 Characterization of the laser cut surface

To evaluate the perpendicularity of the laser cut copper plate, a dedicated design integrating spacers at each wing extremity was processed simultaneously with the exponentially profiled antennas and the TSLW central waveguide. Fig. 5-a attests of an observable slot-opening for a 30 μm slot design after abutting the spacers regions shown in the inset. Fig. 5-b provides a scanning electron microscope (SEM) view of the laser cut surface topography. The first important observation is that structural defects like rounded and beaded edges after matter flowing as well as ejected, re-solidified and welded molten material particles are not observed, contrasting with the use of continuous wave and pulsed lasers down to nanosecond range. Fig. 5-b also reveals two zones of different edge roughness: the upper part labelled '1' in the area of laser beam entrance and the lower one labelled '2' in the area of laser beam exit. Fig. 5-c and 5-d correspond to magnified views of the upper and lower zones, respectively. The upper part reveals a finely micromachining work resulting from material ablation in the so-called regime of optical ablation depth [26]. The lower part exhibits more peaks and pits suggesting that more thermal losses take place as the beam penetrates deeper into the kerf line as a result of hydrodynamic plasma expansion and incoming beam shielding [27]. Although the femtosecond regime does not favor thermally activated matter removal, heat accumulation resulting from a high repetition rate at the bottom of the kerf line can partially activate this ablation mode [28]. The latter regime is consistent with the formation of a crater-like rougher surface as shown in Fig. 5-d. Nevertheless, the overall surface roughness alongside the cutline depth remains in the micron scale, well below the range of terahertz wavelength and is therefore not expected to negatively impact propagation through wave scattering.

Preprints (www.preprints.org) | NOT PEER-REVIEWED | Posted: 26 February 2018 doi:10.20944/preprints201802.0157.v1

Peer-reviewed version available at Photonics 2018, 5, 11; doi:10.3390/photonics5020011

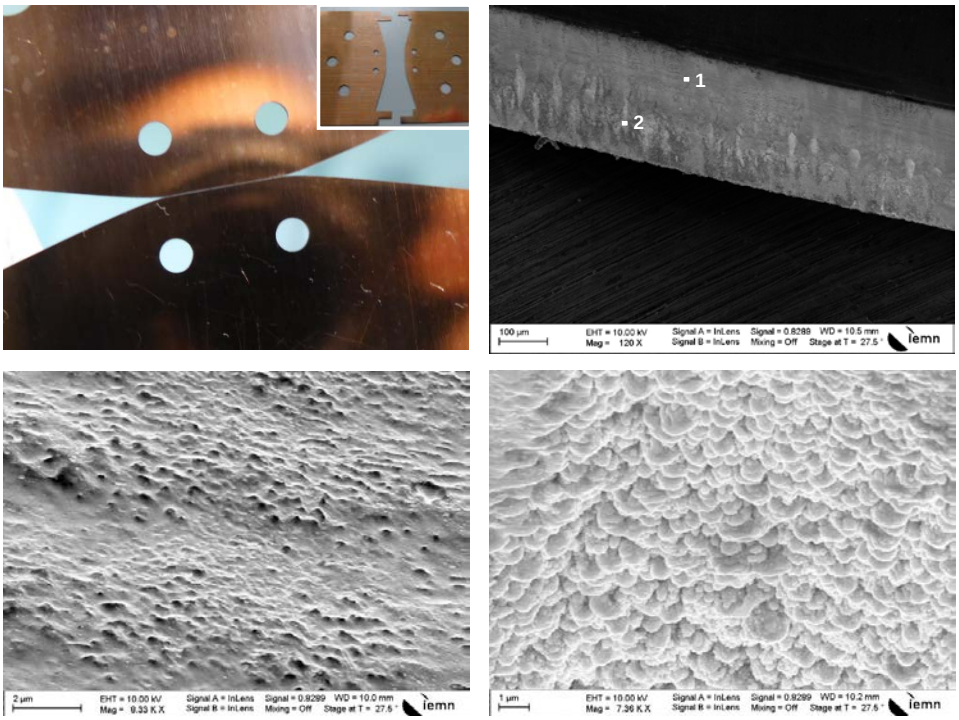

Figure 5. Characterization of the laser cut process **(a)** test of assembly of the two wings showing an observable TSLW slot giving evidence of sidewall perpendicularity. The slot width of 30 µm is determined by two integrated spacers cut at each extremity of the wings as shown in the inset **(b)** SEM view of the laser cut sidewalls, **(c)** magnified view of surface roughness around region 1 **(d)** magnified view of surface roughness around region 2.

4. Characterization

To characterize the device we performed TDS experiments using a Terasmart system from Menlo systems gmbh [16]. We aligned the system (four 50 mm lenses) without any sample or device, and then the collecting lens was moved 10 mm toward the detector to compensate the propagation in the waveguide part and then optimized for the signal. Finally, we aligned the butterfly in order to have the focal plane of both lenses at the entrance and exit of the waveguide. All the system is set in a box flowed by dry nitrogen to avoid parasitic water vapor lines. The raw results are presented in fig 6.

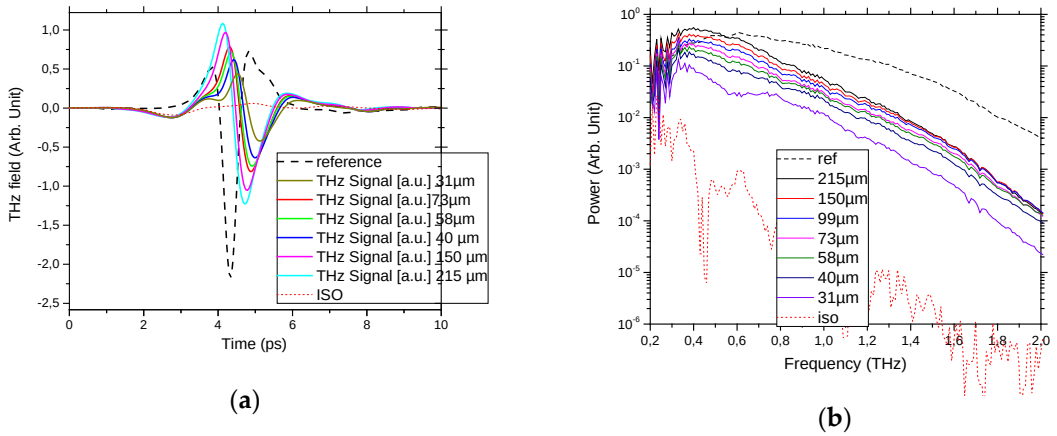

(**a**) (**b**)

Figure 6. Signal recorded from TDS experiments on the butterfly for several w (from 31 µm to 215 µm), the reference is the recorded data without butterfly, the ISO curves are recorded with isopropanol meniscus in the slot (**a**) Time domain signal (**b**) corresponding spectra

Preprints (www.preprints.org) | NOT PEER-REVIEWED | Posted: 26 February 2018 doi:10.20944/preprints201802.0157.v1

Peer-reviewed version available at Photonics 2018, 5, 11; doi:10.3390/photonics5020011

From these results, one can see a small delay (~0.5 ps) between the pulses traveling through the butterfly and the reference one. This delay corresponds to 0.15 mm; that is below to the precision of the lenses positioning. Additionally, the injection/extraction into the Butterfly is shown to be efficient since for low frequencies (below 0.7 THz) the compensation of the diffraction overcome the losses and thus the signal is more important for high w than for the reference. To ensure that the measured signal is actually going through the waveguide of the butterfly, we soaked the waveguide with isopropanol making a meniscus between the two wings (curve denoted ISO in the figures). This shows that most (> 90% for 31 µm and > 98% for 215 µm) of the energy is going through the waveguide, especially for higher frequency as one can see on the spectrum (> 40 dB). Still a parasitic pulse that does not interact with isopropanol can be detected.

4.1 Losses and dispersion

To analyze further our device we calculate the power losses and the dispersion (phase shift with the reference removing the linear term representing the small delay), and show it in fig 7.

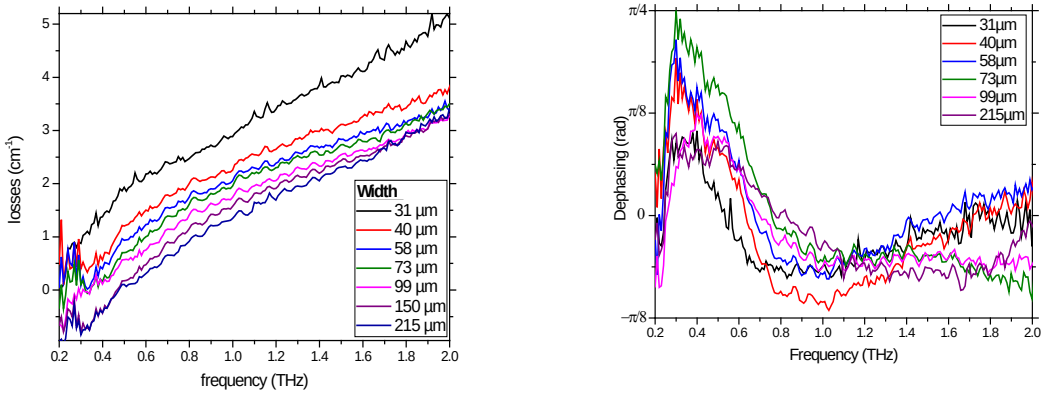

(**a**) (**b**)

Figure 7. (**a**) Power losses for several w, the negative values are due to diffraction; (**b**) dispersion curves for several w.

As stated previously, the compensation of diffraction increases the signal at lower frequency resulting in artificial negative losses. This effect vanishes at frequencies higher than 700 GHz. Thus, the actual losses account for few inverse centimeters, increases with frequency and decrease with the w. The losses shape matches the one computed and shown in fig 2. We attribute the additional losses compared to simulation (a factor ~4) to imperfections in the copper skin depth (< 100 nm @1 THz) leading to additional current path compared to the lossy-metal model. This factor is typical in the THz range [[].

The dispersion is relatively low on the whole spectrum (below π/4). Still the curves show a bump at low frequencies (below 0.7 THz). We attributed this small change to the same effect of diffraction. This has been already seen in similar structures [11]. It is clear from the temporal data that the dispersion is bearable and thus easily reaches the specifications for TDS.

4.2 Benchmarking

Since our primary goal is to measure thin film sample precisely, we benchmarked the butterfly by introducing in the gap a 50 µm-thick Kapton® film. We made this choice due to the highly calibrated thickness and because the refractive index of Kapton had already been carefully measured [29]. The results are shown in fig 8

Preprints (www.preprints.org) | NOT PEER-REVIEWED | Posted: 26 February 2018 doi:10.20944/preprints201802.0157.v1

Peer-reviewed version available at Photonics 2018, 5, 11; doi:10.3390/photonics5020011

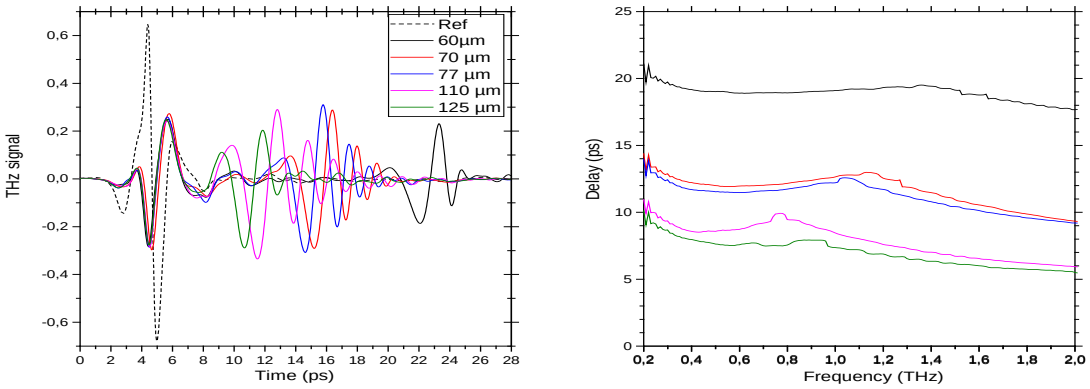

Figure 8. Results of the experiments when inserting a 50 µm thin film layer in the slot of the butterfly. The distance in the legend is the measured slot width w (**a**) Time-domain results (**b**) Corresponding frequency-domain delay calculated by dividing the dephasing from the reference by the frequency.

First, one can see on the time-domain results (fig 8a) that the pulse is delayed when interacting with kapton®. However, a parasitic pulse appears exactly at the same time as the reference pulse. As explained above (see 4.1), this corresponds to the parasitic part of the beam that does not travel through the slot. Then, it is clear from the figure that the wider is the slot the smaller is the delay, this is simply due to the effective index effect in the waveguide. To be quantitative, we extracted the delay (fig 8b) by taking the dephasing of the delayed pulse (by time-domain filtering the parasitic pulse) and divided by the frequency. The results show a very little dispersion, only a small kink in the middle of the band. Since this kink is around a frequency corresponding to a $\lambda/2$ for the corresponding thickness, we attributed this kink to the appearance of the first higher order mode [30].

To confirm our interpretation, we calculated the delay from an effective refractive index model. Considering the capacitor like geometry the effective refractive index can be calculated as:

$$n_{eff}{}^{-2} = \varepsilon_{eff}{}^{-1} = \frac{1}{w}\left(\frac{w_{kapton}}{\varepsilon_{kapton}} + \left(w - w_{kapton}\right)\right) \quad (2)$$

The calculated results are compared to the measurements on fig 9-a. The w error-bars correspond to the uncertainty on the width measurements, the delay error-bars correspond to the propagation of the width's uncertainty on the calculus.

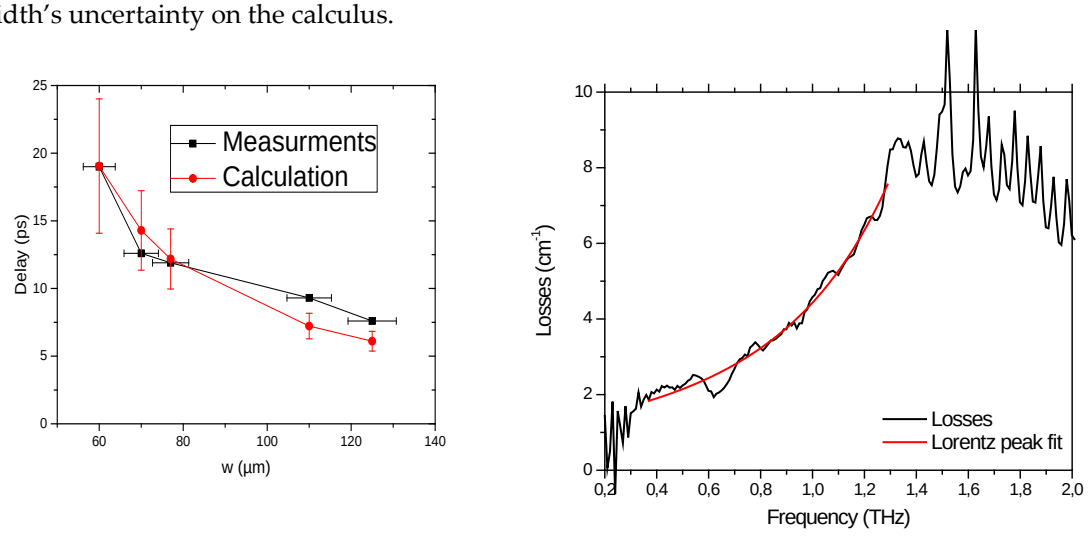

Preprints (www.preprints.org) | NOT PEER-REVIEWED | Posted: 26 February 2018 doi:10.20944/preprints201802.0157.v1

Peer-reviewed version available at Photonics 2018, 5, 11; doi:10.3390/photonics5020011

Figure 9. (a) Comparison of the calculated delay (red dots) versus w with the measured one (back squares). (b) Losses calculated from experimental data at w=60µm fitted with a Lorentz peak function.

This shows a good agreement confirming the interpretations; only the points for higher w are out of the error bars. We attribute this discrepancy to the fact that for lower delays, it was difficult to ensure proper time filtering since the delayed pulse is very close to the parasitic one. To go a step further towards our spectroscopy goals we also show the losses for w = 60 µm on fig 9 b. Since we are probing 10 mm long of a 50 µm thick sample we are able to retrieve extremely low losses at the cm^{-1} level where experiments from the literature were done on 125 µm or 250 µm thick kapton® thin film and this did not allow to measure losses below 10 cm^{-1}. The sensitivity we reached allows us to see the shape of the losses in the spectral range between 0.3 and 1.3 THz showing a super-linear shape as it is often the case. Since this shape could be due to scattering or to the tail of a higher frequency peak, we fitted with four different functions (f^2, f^4, Gaussian and Lorentzian bells) and the best fit we got was for a Lorentz curve centered at 1.95 THz, a width of 0.95 THz and a height of 22 cm^{-1}. These results are fully compatible with the ones in [29] and shows that low absorption peaks can be measured in thin-film. To conclude on Kapton® experiments, the butterfly device enables 1 cm length interaction with a 50 µm thick thin-film sample. As a result, we confirmed the refractive index published in [29] (1.85 +- 0.5). In addition, we were able to measure more precisely the absorption in the spectral range between 0.3 THz and 1.3 THz demonstrating the interest of the butterfly device to measure small absorption features on thin-film sample.

4.3 Test with lactose

In order to show the full capabilities of our device especially regarding biosamples, we performed THz spectroscopy on alpha-lactose monohydrate from sigma Aldrich. This was done in two steps, (1) on a powder sample and (2) on an evaporated lactose solution. For the powder sample we simply fill the slot (w=150 µm) of the butterfly with the purchased powder (volume < 1 µl and a measured mass < 200 µg). For the evaporated liquid sample, we made a saturated solution of lactose in deionized water (200 g/l). Then we filled the slot of the butterfly using a 10 µl micropipette leading to a mass of crystal inside the slot below 2 mg (estimation ~ 200 µg since most of the lactose remained on top of the wings of the butterfly). The spectrum and the reference we obtained are given in fig 10.

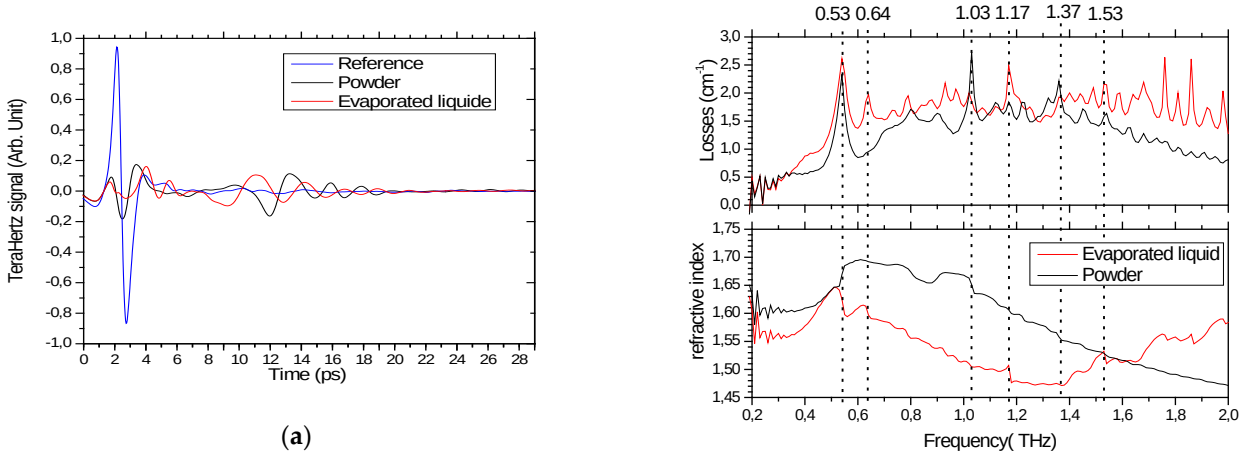

Figure 10. TDS results of experiments on lactose with the butterfly (**a**) time-domain results; (**b**) associated calculated losses and effective refractive index.

First, one can see for the powder and evaporated liquid experiments, that a delayed and broadened pulse (damped oscillation) is recorded. This damped pulse is a signature for spectroscopic lines since it corresponds to the Fourier transform of a Lorentz bell curve (or a sum of Lorentz bell curves). This means we are able, not only, to retrieve the refractive index with the delay, but the absorption lines from our sample. In addition, similarly to the kapton® experiments a parasitic pulse that does not

travel through the sample is recorded (around 2 ps). Thus, to avoid any fake interferences effect we removed the entire signal before 6 ps, before performing the Fourier transform, only keeping the actual data from the sample. From the spectrum, we extracted the effective refractive index and the losses (fig 10 b). First, one can see that the effective refractive index found is slightly below the published one. This is because the slot is not fully filled with lactose. In addition, six peaks with corresponding resonance in the refractive index are pointed out using dotted lines at 0.53, 0.64, 1.03, 1.17, 1.37 and 1.53 THz. From these peaks, the one at 0.64 THz is only seen in evaporated liquid sample and the one at 1.03 only in the powder sample. The peaks at 0.53 THz [10, 31], 1.17 [32, 33] and 1.37 THz [34, 35] are characteristic absorption peaks of for alpha lactose monohydrate. These remarks suggest that the peaks at 1.53 and the one at 1.03 THz may be due to other effects than absorption in material. It could be for instance Mie resonances in crystallites. In fact, there are many other tiny peaks in the spectra, especially in the evaporated liquid one, which we interpreted as such. To conclude, the use of the butterfly allowed us to perform THz spectroscopy on minute powder sample (< 1µl) and evaporated liquid sample (<10µl of liquid) and we were able to find back the peaks from literature. However, we will need to repeat the experiments to make the difference between absorption peaks and Mie resonance peaks.

5. Conclusion

In this paper, we designed a butterfly device made of two antennas and a slot waveguide with the goal to concentrate the field from a TDS experiments in the small volume. To follow the specific constraints of being low-losses, low-dispersion and to have the slot of the waveguide accessible, we used a 2D geometry device fabricated thanks to laser cutting of copper plates. Then, we characterized the butterfly using TDS and showed that their properties fulfilled the requirements for spectroscopy on biosamples in the 0.2-2 THz range. Consequently, we were able to perform broadband TDS spectroscopy of a 50 µm-thick Kapton® film and to detect small absorption feature up to 2 THz. Finally, we used the butterfly on simulated biosamples (lactose powder and lactose solution). In both cases, we measured the typical peak at 0.53 THz on µl sample. Still, several improvements or modifications are possible like changing the length of the waveguide or improving parallelism to reach waveguide width as thin as 10 µm. We think that the already demonstrated performances of the butterfly device open the path to many future experiments on other biosamples such as proteins, DNA, RNA, or other macromolecules and thus consist on a step forward for THz Biophotonics spectroscopy.

Acknowledgments: This work was partially supported by: i) the international chair of excellence “ThOTroV” from region “Hauts-de-France” ii) the French government through the National Research Agency (ANR) under programs PIA EQUIPEX LEAF ANR-11-EQPX-0025 and ExCELSiOR ANR 11-EQPX-0015 and iii) the French RENATECH network on micro and nanotechnologies.

6. References

1. [1] Christian Koos, Philipp Vorreau, Thomas Vallaitis, Pieter Dumon, Wim Bogaerts, Roel Baets, Bweh Esembeson, Ivan Biaggio, Tsuyoshi Michinobu, François Diederich, et al. All-optical high-speed signal processing with silicon–organic hybrid slot waveguides. *Nature Photonics*, 3(4):216–219, 2009.
2. [2] Clément Sieutat, Romain Peretti, Jean-Louis Leclercq, Pierre Viktorovitch, and Xavier Letartre. Strong confinement of light in low index materials: the photon cage. *Opt. Express*, 21(17):20015–20022, Aug 2013.
3. [3] Nicolas Descharmes, Ulagalandha Perumal Dharanipathy, Zhaolu Diao, Mario Tonin, and Romuald Houdré. Observation of backaction and self-induced trapping in a planar hollow photonic crystal cavity. *Phys. Rev. Lett.*, 110:123601, Mar 2013.
4. [4] Stefan A Maier and Harry A Atwater. Plasmonics: Localization and guiding of electromagnetic energy in metal/dielectric structures. *Journal of Applied Physics*, 98(1):011101, 2005.
5. [5] Romain Quidant and Christian Girard. Surface-plasmon-based optical manipulation. *Laser & Photonics Reviews*, 2(1-2):47–57, 2008.

6. [6] Ye Pu, Rachel Grange, Chia-Lung Hsieh, and Demetri Psaltis. Nonlinear optical properties of core-shell nanocavities for enhanced second-harmonic generation. *Physical review letters*, 104(20):207402, 2010.
7. [7] Bernd M Fischer, Hanspeter Helm, and Peter Uhd Jepsen. Chemical recognition with broadband thz spectroscopy. *Proceedings of the IEEE*, 95(8):1592–1604, 2007.
8. [8] E Castro-Camus and MB Johnston. Conformational changes of photoactive yellow protein monitored by terahertz spectroscopy. *Chemical Physics Letters*, 455(4):289–292, 2008.
9. [9] Stefan Mastel, Mark B. Lundeberg, Pablo Alonso-González, Yuanda Gao, Kenji Watanabe, Takashi Taniguchi, James Hone, Frank H. L. Koppens, Alexey Y. Nikitin, and Rainer Hillenbrand. Terahertz nanofocusing with cantilevered terahertz-resonant antenna tips. *Nano Letters*, 17(11):6526–6533, 2017. PMID: 29035061.
10. [10] Markus Walther, Mark R. Freeman, and Frank A. Hegmann. Metal-wire terahertz time-domain spectroscopy. *Applied Physics Letters*, 87(26):261107, 2005.
11. [11] Rajind Mendis and Daniel Grischkowsky. Undistorted guided-wave propagation of subpicosecond terahertz pulses. *Optics letters*, 26(11):846–848, 2001.
12. [12] Martin Van Exter, Ch Fattinger, and D Grischkowsky. Terahertz time-domain spectroscopy of water vapor. *Optics letters*, 14(20):1128–1130, 1989.
13. [13] D Grischkowsky, Søren Keiding, Martin Van Exter, and Ch Fattinger. Far-infrared time-domain spectroscopy with terahertz beams of dielectrics and semiconductors. *JOSA B*, 7(10):2006–2015, 1990.
14. [14] N. Laman, S. Sree Harsha, D. Grischkowsky, and Joseph S. Melinger. High-resolution waveguide thz spectroscopy of biological molecules. *Biophysical Journal*, 94(3):1010 – 1020, 2008.
15. [15] Alisha J Shutler and D Grischkowsky. Gap independent coupling into parallel plate terahertz waveguides using cylindrical horn antennas. *Journal of Applied Physics*, 112(7):073102, 2012.
16. [16] http://www.menlosystems.com/en/products/thz-time-domain-solutions/terasmart-terahertz-spectrometer/.
17. [17] H. Oraizi and S. Jam. Optimum design of tapered slit antenna profile. *IEEE Transactions on Antennas and Propagation*, 51(8):1987–1995, Aug 2003.
18. [18] S. B. Cohn. Slit line on a dielectric substrate. *IEEE Transactions on Microwave Theory and Techniques*, 17(10):768–778, Oct 1969.
19. [19] Charles Vassallo. *Théorie des guides d'ondes électromagnétiques*, volume 1. Eyrolles, 1985.
20. [20] T. Kitazawa, Y. Fujiki, Y. Hayashi, and M. Suzuki. Slit line with thick metal coating (short papers). *IEEE Transactions on Microwave Theory and Techniques*, 21(9):580–582, Sep 1973.
21. [21] T. Kitazawa, Y. Hayashi, and M. Suzuki. Analysis of the dispersion characteristic of slit line with thick metal coating. *IEEE Transactions on Microwave Theory and Techniques*, 28(4):387–392, Apr 1980.
22. [22] Georgios Veronis and Shanhui Fan. Guided subwavelength plasmonic mode supported by a slit in a thin metal film. *Opt. Lett.*, 30(24):3359–3361, Dec 2005.
23. [23] https://www.cst.com/.
24. [24] Hamid Pahlevaninezhad, Barmak Heshmat, and Thomas Edward Darcie. Efficient terahertz slot-line waveguides. *Opt. Express*, 19(26):B47–B55, Dec 2011.
25. [25] Sanjay Mishra and Vinod Yadava. Laser beam micromachining (lbmm) ? a review. *Optics and Lasers in Engineering*, 73(Supplement C):89 – 122, 2015.
26. [26] C Momma, S Nolte, B N. Chichkov, F v. Alvensleben, and A Tünnermann. Precise laser ablation with ultrashort pulses. *Applied Surface Science*, 109-110(Supplement C):15 – 19, 1997.
27. [27] S. Nolte, C. Momma, H. Jacobs, A. Tünnermann, B. N. Chichkov, B. Wellegehausen, and H. Welling. Ablation of metals by ultrashort laser pulses. *J. Opt. Soc. Am. B*, 14(10):2716–2722, Oct 1997.
28. [28] Rudolf Weber, Thomas Graf, Christian Freitag, Anne Feuer, Taras Kononenko, and Vitaly I. Konov. Processing constraints resulting from heat accumulation during pulsed and repetitive laser materials processing. *Opt. Express*, 25(4):3966–3979, Feb 2017.
29. [29] Paul D. Cunningham, Nestor N. Valdes, Felipe A. Vallejo, L. Michael Hayden, Brent Polishak, Xing-Hua Zhou, Jingdong Luo, Alex K.-Y. Jen, Jarrod C. Williams, and Robert J. Twieg. Broadband terahertz characterization of the refractive index and absorption of some important polymeric and organic electro-optic materials. *Journal of Applied Physics*, 109(4):043505–043505–5, 2011.
30. [30] Jyh-Wen Sheen and Yu-De Lin. Propagation characteristics of the slotline first higher order mode. *IEEE transactions on microwave theory and techniques*, 46(11):1774–1781, 1998.

31. [31] D.G. Allis, A.M. Fedor, T.M. Korter, J.E. Bjarnason, and E.R. Brown. Assignment of the lowest-lying thz absorption signatures in biotin and lactose monohydrate by solid-state density functional theory. *Chemical Physics Letters*, 440(4):203 – 209, 2007.
32. [32] Withawat Withayachumnankul, Bernd M. Fischer, and Derek Abbott. Material thickness optimization for transmission-mode terahertz time-domain spectroscopy. *Opt. Express*, 16(10):7382–7396, May 2008.
33. [33] B. B. Jin, Z. X. Chen, Z. Li, J. L. Ma, R. Fu, C. H. Zhang, J. Chen, and P. H. Wu. Mode assignment of terahertz spectrum of alpha-lactose monohydrate. In *2009 34th International Conference on Infrared, Millimeter, and Terahertz Waves*, pages 1–2, Sept 2009.
34. [34] J Axel Zeitler, Karin Kogermann, Jukka Rantanen, Thomas Rades, Philip F Taday, Michael Pepper, Jaakko Aaltonen, and Clare J Strachan. Drug hydrate systems and dehydration processes studied by terahertz pulsed spectroscopy. *International journal of pharmaceutics*, 334(1):78–84, 2007.
35. [35] Yoichi Kawada, Takashi Yasuda, Atsushi Nakanishi, Koichiro Akiyama, and Hironori Takahashi. Single-shot terahertz spectroscopy using pulse-front tilting of an ultra-short probe pulse. *Opt. Express*, 19(12):11228–11235, Jun 2011.